CONFIDENTIAL

Copy
RM L54K12

340

CASE FILE
COPY

RESEARCH MEMORANDUM

TRANSONIC LONGITUDINAL AERODYNAMIC EFFECTS OF SWEEPING UP THE REAR OF THE FUSELAGE OF A ROCKET-PROPELLED AIRPLANE MODEL HAVING NO HORIZONTAL TAIL

By James H. Parks

Langley Aeronautical Laboratory
Langley Field, Va.

CLASSIFICATION CHANGED TO UNCLASSIFIED
AUTHORITY: NACA RESEARCH ABSTRACT NO. 122
EFFECTIVE DATE: NOVEMBER 8, 1957 WHL

CLASSIFIED DOCUMENT

This material contains information affecting the National Defense of the United States within the meaning of the espionage laws, Title 18, U.S.C., Secs. 793 and 794, the transmission or revelation of which in any manner to an unauthorized person is prohibited by law.

NATIONAL ADVISORY COMMITTEE
FOR AERONAUTICS

WASHINGTON
January 20, 1955

CONFIDENTIAL

NATIONAL ADVISORY COMMITTEE FOR AERONAUTICS

RESEARCH MEMORANDUM

TRANSONIC LONGITUDINAL AERODYNAMIC EFFECTS OF SWEEPING UP THE REAR OF THE FUSELAGE OF A ROCKET-PROPELLED AIRPLANE MODEL HAVING NO HORIZONTAL TAIL

By James H. Parks

SUMMARY

Results are presented of a free-flight investigation employing two rocket-propelled airplane models to determine the effects of fuselage upsweep on the transonic longitudinal aerodynamic characteristics for the horizontal-tail-off condition. Both models had 45° swept wings with the only geometric difference being the upsweep of the rear of the fuselage center line.

Sweeping-up the fuselage resulted in lower lift-curve slopes particularly at low positive angles of attack and generally moved the aerodynamic-center location rearward. The upswept fuselage configuration exhibited a greater transonic trim change and markedly greater drag coefficients at Mach numbers above about 0.95. Local downflow measurements indicate similar effects for both fuselages on local flow angles at a representative horizontal-tail location.

INTRODUCTION

A general research program has been conducted at the National Advisory Committee for Aeronautics to determine, by means of rocket-propelled models in free flight, the effects of various empennage designs on the longitudinal aerodynamic characteristics of complete airplane configurations at transonic speeds. The results of tests which employed horizontal tails mounted in three different positions on a 45° swept wing combined with a parabolic body of revolution fuselage have been reported previously in references 1 and 2. Presented herein are the results of the test for the horizontal-tail-off condition. Also presented are the results of a test using a similar wing-fuselage combination which had the rear of the fuselage upswept in line with current design practice of providing additional ground clearance for the landing condition.

The flight tests were conducted at the Langley Pilotless Aircraft Research Station at Wallops Island, Va.

SYMBOLS

b	wing span, 3.25 ft
c	chord, ft
$\bar{c}$	mean aerodynamic chord, $\frac{\int_0^{b/2} c^2 dy}{\int_0^{b/2} c\, dy}$, 0.851 ft
g	gravitational acceleration, ft/sec^2
q	dynamic pressure, lb/sq ft
I_Y	moment of inertia in pitch, slug-ft^2
M	Mach number
S	wing area, 2.78 sq ft
V	velocity, ft/sec
W	weight of model, lb
a_n/g	normal acceleration, positive up
α	angle of attack, deg
θ	angle of pitch, radians
C_N	normal-force coefficient, $\frac{Wa_n}{Sqg}$
C_L	lift coefficient, $C_N \cos \alpha$
C_m	pitching moment about center of gravity, $\frac{\text{Pitching moment}}{qS\bar{c}}$

$\dot{\alpha}$ rate of change of angle of attack, $\frac{1}{57.3}\frac{d\alpha}{dt}$, radians/sec

q pitching velocity, $\frac{d\theta}{dt}$, radians/sec

$C_{m_q} + C_{m_{\dot{\alpha}}}$ damping-in-pitch parameter, $C_{m_{q\bar{c}/2V}} + C_{m_{\dot{\alpha}\bar{c}/2V}}$

Symbols used as subscripts indicate the derivative of the quantity with respect to the subscript, for example, $C_{L_\alpha} = \frac{dC_L}{d\alpha}$

MODELS AND INSTRUMENTATION

Models

Three-view drawings of the models are shown as figure 1. Details of construction are given in reference 1. Briefly, the models are constructed primarily of laminated mahogany with metal plates incorporated in the wings for additional stiffness and rigidity.

The models will hereinafter be referred to as symmetric fuselage (fig. 1(a)) and unsymmetric fuselage (fig. 1(b)). The symmetric fuselage is the basic parabolic body of revolution used in references 1 and 2, the ordinates of which are tabulated in reference 1. The unsymmetric fuselage was designed by making the top of the fuselage parallel to the original fuselage center line rearward of the maximum diameter station and retaining the original fuselage ordinates in planes normal to the original fuselage center line.

The wings incorporated 45° sweepback of the c/4 line, were of aspect ratio 4.0, and had NACA 65A006 airfoil sections in the streamwise direction. The vertical tails were also swept back 45° and had similar airfoil sections but of 8 percent thickness. Pertinent mass characteristics of the models are as follows:

	Symmetric fuselage	Unsymmetric fuselage
Weight, lb	44.00	44.75
I_Y, slug-ft^2	2.825	2.854
Center-of-gravity location, percent $\bar{c}$	-14.4	-10.2

Instrumentation

The models were equipped with NACA four-channel telemeters which transmitted continuous records of normal acceleration, angle of attack, total pressure, and a local flow direction at a position corresponding, on the symmetric fuselage, to the horizontal-tail location used in reference 1.

Ground instrumentation included tracking radar, to determine flight path in space, and a Doppler velocimeter unit for additional velocity information. A radiosonde was released immediately after model launchings to determine atmospheric conditions at altitude. Also motion-picture coverage was used to determine general flight behavior during the early portion of the flight.

TEST AND ANALYSIS TECHNIQUES

The models were accelerated to maximum velocity by ABL Deacon rocket motors. A model-booster combination is shown on the launching platform at the launching angle of 60° elevation in figure 2. The vertically thrusting pulse-rocket installation used to produce longitudinal oscillations is described in reference 1. Each pulse rocket had a total impulse of approximately 8 pound-seconds and a burning time of about 0.08 second.

Detailed discussions of the general data reduction techniques are presented in reference 3. The particular applications to the present technique are presented in reference 1. Briefly, C_{L_α} data are obtained by measuring slopes on plots of C_L against α, C_{m_α} from periods of free oscillations, and $C_{m_q} + C_{m_{\dot{\alpha}}}$ from the rate of decay of free oscillations.

ACCURACY

Accuracy of this type of investigation is discussed in detail in references 1 and 3. For the particular instrumentation used, the absolute accuracy in C_L is ± 0.01 at $M = 1.20$ and ± 0.02 at $M = 0.80$ with considerably better accuracy in incremental values. The angle of attack and local flow angle are believed correct within $\pm 0.30^\circ$ and Mach number is estimated to be accurate within ± 0.02 at $M = 1.00$. It might be noted that the lift coefficient is defined as a function of normal force only (see section entitled "Symbols") since $C_N \approx C_L$ near $\alpha = 0$.

The accuracy of drag data as obtained from velocimeter data for nonmaneuvering models is discussed in reference 4. For the maneuvering models in the present tests it is believed that the drag-coefficient levels are correct within ±0.002 at supersonic and subsonic speeds. Near M = 1.00 the values are probably somewhat less reliable.

RESULTS AND DISCUSSIONS

The scales of the tests are shown as Reynolds numbers, based on $\bar{c}$, plotted against Mach number in figure 3. Also shown in figure 3 are the dynamic pressures as a function of Mach number. It should be pointed out here that motion pictures of the flight of the unsymmetric fuselage indicated Dutch rolling motions of appreciable amplitude coincident with the pulse-rocket induced longitudinal oscillations. Results of reference 5 indicate that the longitudinal motions for this model may be affected by the Dutch roll through inertial cross coupling. While no measurements of the lateral motions were made, it is felt that the effects on the longitudinal data are small but should be considered in the data comparison.

Lift

Basic lift-curve plots for the various Mach numbers are presented in figures 4 and 5. It should be pointed out here that the preponderance of the data is in the angle-of-attack range between $\pm 2^\circ$ and is therefore only directly applicable to the low-lift condition.

The lift curves for the symmetric fuselage (fig. 4) are linear, whereas the lift curves for the unsymmetric fuselage become nonlinear in the angle-of-attack range from 0° to 2°. The symmetric-fuselage results are essentially symmetric about zero angle of attack whereas positive values of lift coefficient are indicated for the unsymmetric fuselage at zero angle of attack. The magnitude of these lift coefficients at $\alpha = 0^\circ$ decreased from about 0.04 at M = 0.71 to approximately 0.01 at M = 1.32.

The slopes of the lift curves are shown in figure 6. Since the relatively flexible wings are subject to aeroelastic losses, particularly at the higher Mach numbers, the flexibility data of reference 1 were used to determine the order of magnitude of these losses. Only the symmetric-fuselage data are shown corrected to the rigid wing case (fig. 6(a)) because the dynamic pressure data of figure 3 indicate that the losses should be essentially the same for both configurations. The order of magnitude and variation with Mach number of the symmetric-fuselage lift-curve data, with this aeroelastic correction applied, are in good general agreement with the summary data of reference 6.

The degree of nonlinearity present in the unsymmetric-fuselage lift-curve data is evident in figure 6(b). At Mach numbers below 0.95, the values at the negative angles of attack are approximately 0.025 higher than for comparable values at the low positive angles of attack. The linearity indicated at Mach numbers above 1.19 may be due in part to the limited ranges of the data available at these Mach numbers (fig. 5). Comparison of the two configurations in figure 6(b) indicates that sweeping up the rear of the fuselage has reduced the lifting capabilities throughout the Mach number and angle-of-attack ranges covered.

The differences in lift noted between the two configurations are compatible with the results of reference 7 wherein the effects of changing from a cylindrical afterbody to one having a symmetrically boattailed afterbody are presented in detail. Differences are shown to arise from changes in the wing loading due to the differences in wing-fuselage interference and from changes in the afterbody loading. Although these data are not directly applicable in a quantitative sense, it is indicated that, relative to the symmetric fuselage, the unsymmetric fuselage is slightly more negatively loaded over the wing and over the fuselage in the vicinity of the wing but has a region of relatively high positive loading near the fuselage base.

Apparently the positive loading predominates at $\alpha = 0^\circ$ to produce the increment of positive lift noted for the unsymmetric fuselage in the present tests. Since the wind-tunnel data further indicate that the wing-fuselage interference effects remain essentially constant throughout the Mach number range, this positive loading must decrease with increasing speed as indicated by the decay in this positive lift increment noted previously. As the angle of attack is varied, the wing becomes of primary importance and the regions of more negative loading predominate as indicated by the lower lift-curve slopes. The reasons for the particularly large effect at low positive angles of attack are not known and the wind-tunnel data are not sufficiently definite to offer any explanation.

Static Stability

The static stability parameters for the symmetric fuselage are summarized in figure 7. Similar data for the unsymmetric fuselage are presented in figure 8. More complete period data are available for the unsymmetric fuselage, but the data show somewhat greater scatter probably as a result of nonlinearities (see section entitled "Lift"). These nonlinearities are not defined in the present data.

The values of C_{m_α} presented represent the faired lines shown in the period data and thus are to some extent average values particularly for the unsymmetric fuselage. Values for both configurations are generally of the same order of magnitude.

The aerodynamic-center location for the symmetric fuselage as shown in figure 7 is somewhat farther forward than the results of reference 6 indicate at transonic speeds. This effect, particularly at the higher Mach numbers, is due to the more flexible wing construction used in the present investigation. An increment of forward movement arising from this aeroelastic effect was determined by using the method of reference 8. The application of this correction brings the data into good general agreement with the results of reference 6.

The aerodynamic-center locations shown for the unsymmetric fuselage reflect the nonlinear lift-curve slopes discussed previously. If the flexibility effects are assumed to be about the same for both configurations, the more rearward aerodynamic-center locations shown for the unsymmetric fuselage indicate that the total effect of fuselage upsweep is to move the center of pressure on the fuselage alone rearward. This is particularly true when it is considered that the unloading effect of wing-fuselage interference noted previously should tend to reduce the static stability of the unsymmetric fuselage. This increment of rearward aerodynamic-center location is generally about 7 percent $\bar{c}$ at negative angles of attack except for small regions above and below $M = 1.0$. As in the lift case, the reasons for the larger increments shown at low positive angles of attack are not known.

Dynamic Stability

The dynamic stability parameters for both configurations are presented in figure 9. In both cases, the general level of damping-moment coefficient is of the same order of magnitude above $M = 1.0$. At lower Mach numbers, the unsymmetric-fuselage data are more erratic and the value of damping-moment coefficient is near zero at $M \approx 0.75$.

The low subsonic damping-moment coefficient indicated for the unsymmetric fuselage may be due in part to the use of the higher lift-curve slopes in the calculations. Since the measured value of time to half amplitude includes both moment and lift damping, nonlinear lift-curve slopes preclude accurate isolation of the damping-moment coefficient in the present analysis. Also the inertial cross coupling mentioned previously could be expected to affect the damping data particularly. For these reasons, the level indicated by the symmetric fuselage is believed the more realistic.

Trim

The variations of trim lift coefficients and trim angles of attack over the Mach number ranges are shown in figure 10. The changes in trim at transonic speeds while generally nose-up for both configurations are

appreciably larger for the unsymmetrical fuselage. Because of the nonlinearities in lift, this is more evident in the angle-of-attack data. In both instances the variation in trim with Mach number is mild with no abrupt changes. While the trim comparisons are strictly valid only for the same center-of-gravity location, the error introduced by the small difference ($0.042\bar{c}$) in the present tests introduces a negligible error.

Since an appreciable portion of the trim changes is due to the drag of the vertical tail, it is of interest to look at the pitching-moment coefficients at zero angle of attack which are shown in figure 11. The total pitching-moment coefficient at zero angle of attack was obtained by extrapolating linearly the trim data by using C_{m_α} values. The increment of pitching-moment coefficient due to the vertical tail was calculated by using the data of reference 6 and increasing the pressure drag by a factor of $(t/c)^{5/3}$. The greater increment shown for the unsymmetric fuselage is due to the higher location of the vertical tail relative to the model center-of-gravity position.

For these reasons, it would be expected that the symmetric fuselage would trim at a small positive angle of attack. The small negative trim values indicated at $M < 1.05$ (fig. 10) are believed to be the result of the absolute accuracy of the data (see section entitled "Accuracy") and small deviations in model construction. The trend over the Mach number range should be relatively unaffected by those effects.

For the symmetric-fuselage case, it may be assumed that the wing-fuselage combination would have zero pitching-moment coefficient at zero angle of attack. Thus the difference between the total pitching-moment coefficient and the increment of pitching-moment coefficient due to the vertical tail (fig. 11) should be indicative of unaccounted-for asymmetries inherent in both models. The increased nose-down pitching-moment coefficients shown in figure 11(c) for the unsymmetric fuselage are believed due to sweeping up the rear of the fuselage. These wing-fuselage pitching-moment coefficients are generally less at supersonic speeds than at subsonic speeds with a value of -0.030 at $M = 0.90$ and about -0.017 at $M = 1.30$. These negative increments are associated with the increments of positive lift at zero angle of attack noted previously and agree generally in that both decrease with increasing Mach number. The more rapid decrease in lift with increasing speed indicates the possibility of a rearward movement of the afterbody loading; however, these data are not complete enough to verify this.

A similar nose-down pitching moment was noted for the model of reference 9 wherein a less severe amount of upsweep was incorporated in the fuselage.

Drag

The drag variations with Mach number at trim lift conditions are presented for both configurations in figure 12. Although the levels of the drag coefficients appear high in comparison with the results of reference 6, they appear reasonable when the much larger fuselage frontal area to wing area ratio (approximately 0.12 in the present tests) and the comparatively thick (8 percent) vertical tail are considered. It is indicated that an appreciable afterbody pressure drag penalty of the order of 7 percent is incurred at low supersonic speeds when the entire boattailing in the plane of symmetry is restricted to the underside of the fuselage.

Local Flow Angles at the Tail

Local angles of attack measured at a representative horizontal-tail location for the respective model trim conditions are shown in figure 13. Also shown are the contributions of local flow angles obtained by subtracting total local angles from the model angle of attack. The general shapes of the curves are similar with comparatively large increases starting near $M = 0.85$, a general leveling off near $M = 1.00$, and then decreasing again near $M = 1.2$. The symmetrical fuselage indicates the more abrupt changes and higher levels up to $M \approx 1.3$.

Since wing downwash should be negligible at model zero angle of attack, local flow angles for this condition as indicated by the faired lines of figures 14 and 15 are also shown in figure 13. Though some changes in magnitude are shown, the general variations with Mach number are unchanged. The main difference noted between the two models is near $M = 1.3$ where the values for the symmetric fuselage decrease to approximately the subsonic level whereas the values for the unsymmetric fuselage remain near the relatively high transonic level after supersonic flow is established. It is of interest to note that the maximum level for the symmetric fuselage, approximately 6°, is about the same as the slope of the top of the fuselage immediately below the measuring vane. It is believed that this fuselage slope is the primary factor in inducing the flow angularity for the symmetric fuselage whereas the region of positive lift noted in the section entitled "Lift" induces the similar flow angularity shown for the unsymmetric fuselage.

The variations of downflow angle with angle of attack during the pulse rocket-induced oscillations are shown in figures 14 and 15. These data are corrected for the effects of pitching velocity. The scatter evident in the data is partially attributable to the proximity of the fuselage to the measuring vane.

The straight line fairings shown in figures 14 and 15 are represented as downflow slopes in figure 16 as a function of Mach number. Generally the rate of change of downflow increases with increasing Mach numbers for the symmetrical fuselage, whereas the average values for the unsymmetric fuselage tend to decrease with increasing Mach number. Geometric considerations made direct comparisons difficult, but the results of reference 10 generally substantiate the strong influence of the fuselage on local downflow shown herein.

Though these downflow effects are probably localized, the effect can be appreciable. The model of reference 1 had a horizontal-tail location corresponding to the symmetric-fuselage vane location in the present tests. With a tail setting of 2° trailing edge down, an effective angle of attack of the order of -1° was induced over the horizontal tail at $M = 1.11$. Also the shape of the trim curve is quite similar to the present symmetric-fuselage downflow curve.

The results of reference 11, wherein a vane representative of a full-size horizontal tail was used, also show appreciable effective tail angle of attack at model zero angle of attack.

CONCLUDING REMARKS

A flight test investigation at transonic speeds was made using rocket-propelled models of two horizontal-tail-off configurations to determine the respective longitudinal aerodynamic characteristics at low lift. One model had symmetric boattailing whereas the other incorporated upsweep of the rear of the fuselage.

Nonlinearities in the unsymmetric-fuselage data make quantitative comparisons difficult but sweeping up the rear of the fuselage generally reduced the lift-curve slope with the decrease being particularly pronounced at low positive angles of attack. The nonlinearities are not easily identified in the stability data; however, the average values presented indicate a general rearward movement of the aerodynamic center as a result of sweeping up the fuselage.

The unsymmetric fuselage exhibited a considerably larger transonic trim change in the nose-up direction than did the symmetric fuselage. The trim changes were mild with no abrupt variations in either case. An appreciable increase in drag is associated with the unsymmetric fuselage at Mach numbers from about 0.95 to the test limit of 1.35.

Local downflow measurements indicate similar effects for both fuselages on local downflow at a representative horizontal-tail location.

Langley Aeronautical Laboratory,
National Advisory Committee for Aeronautics,
Langley Field, Va., October 29, 1954.

REFERENCES

1. Parks, James H., and Kehlet, Alan B.: Longitudinal Stability, Trim, and Drag Characteristics of a Rocket-Propelled Model of an Airplane Configuration Having a 45° Sweptback Wing and an Unswept Horizontal Tail. NACA RM L52F05, 1952.

2. Parks, James H., and Kehlet, Alan B.: Longitudinal Stability and Trim of Two Rocket-Propelled Airplane Models Having 45° Sweptback Wings and Tails With the Horizontal Tail Mounted in Two Positions. NACA RM L53J12a, 1953.

3. Gillis, Clarence L., Peck, Robert F., and Vitale, A. James: Preliminary Results From a Free-Flight Investigation at Transonic and Supersonic Speeds of the Longitudinal Stability and Control Characteristics of an Airplane Configuration With a Thin Straight Wing of Aspect Ratio 3. NACA RM L9K25a, 1950.

4. Wallskog, Harvey A., and Hart, Roger G.: Investigation of the Drag of Blunt-Nosed Bodies of Revolution in Free Flight at Mach Numbers From 0.6 to 2.3. NACA RM L53D14a, 1953.

5. Parks, James H.: Experimental Evidence of Sustained Coupled Longitudinal and Lateral Oscillations From a Rocket-Propelled Model of a 35° Swept Wing Airplane Configuration. NACA RM L54D15, 1954.

6. Donlan, Charles J., Myers, Boyd C., II, and Mattson, Axel T.: A Comparison of the Aerodynamic Characteristics at Transonic Speeds of Four Wing-Fuselage Configurations As Determined From Different Test Techniques. NACA RM L50H02, 1950.

7. Loving, Donald L.: The Effect of a Change in Body Shape on the Loading of a 45° Sweptback Wing-Body Combination at Transonic Speeds. NACA RM L54B09, 1954.

8. Vitale, A. James: Effects of Wing Elasticity on the Aerodynamic Characteristics of an Airplane Configuration Having 45° Sweptback Wings As Obtained From Free-Flight Rocket-Model Tests at Transonic Speeds. NACA RM L52L30, 1953.

9. Mitcham, Grady L., Stevens, Joseph E., and Norris, Harry P.: Aerodynamic Characteristics and Flying Qualities of a Tailless Triangular-Wing Airplane Configuration As Obtained From Flights of Rocket-Propelled Models at Transonic and Low Supersonic Speeds. NACA RM L9L07, 1950.

10. Osborne, Robert S.: A Transonic-Wing Investigation in the Langley 8-Foot High-Speed Tunnel at High Subsonic Mach Numbers and at a Mach Number of 1.2. Wing-Fuselage Configuration Having a Wing of 45° Sweepback, Aspect Ratio 4, Taper Ratio 0.6, and NACA 65A006 Airfoil Section. NACA RM L50H08, 1950.

11. Weil, Joseph, and Goodson, Kenneth W.: Aerodynamic Characteristics of a Wing With Quarter-Chord Line Swept Back 45°, Aspect Ratio 4, Taper Ratio 0.6, and NACA 65A006 Airfoil Section. Transonic Bump Method. NACA RM L9A21, 1949.

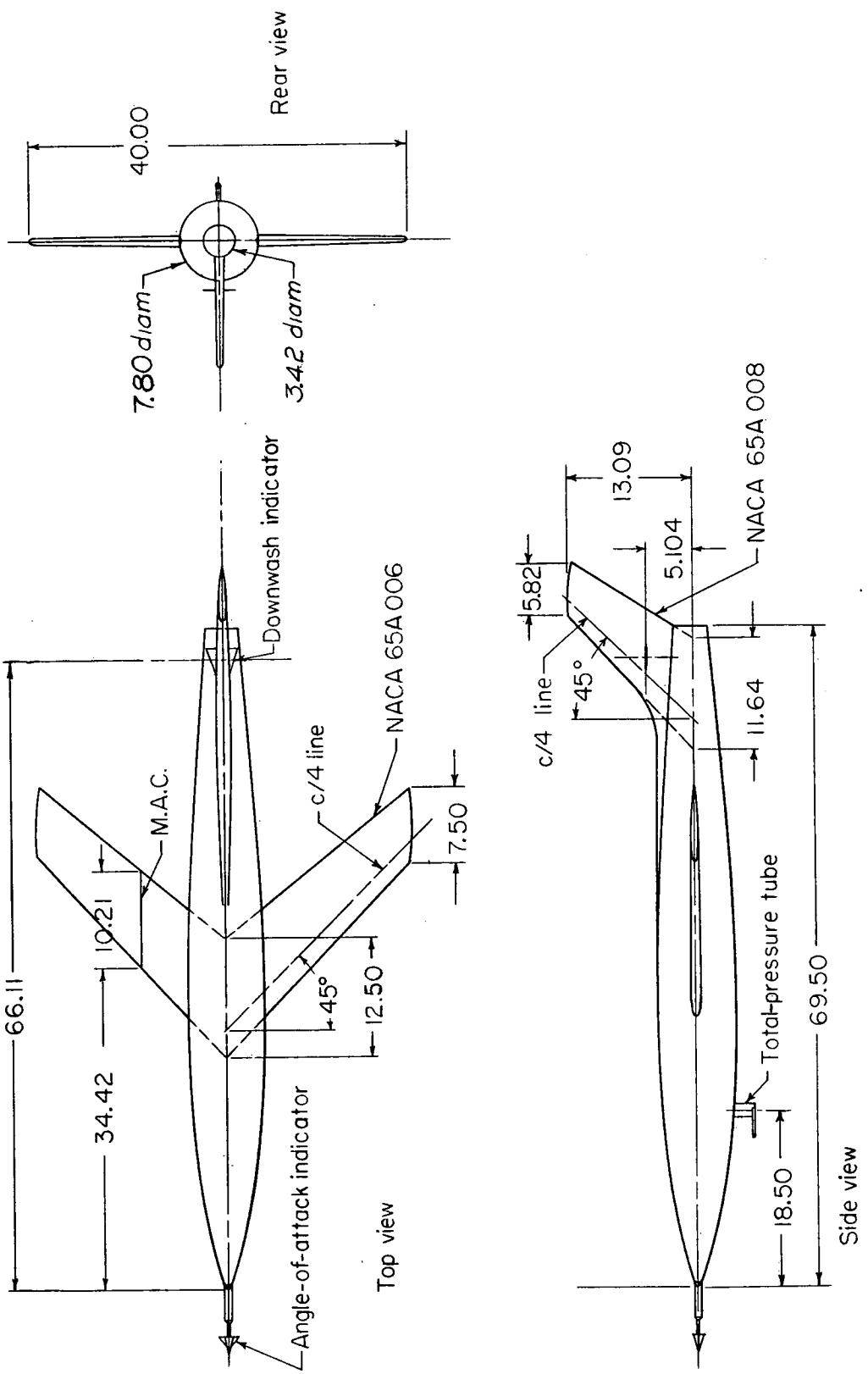

(a) Symmetric fuselage model.

Figure 1.- General arrangement of the models. All dimensions in inches.

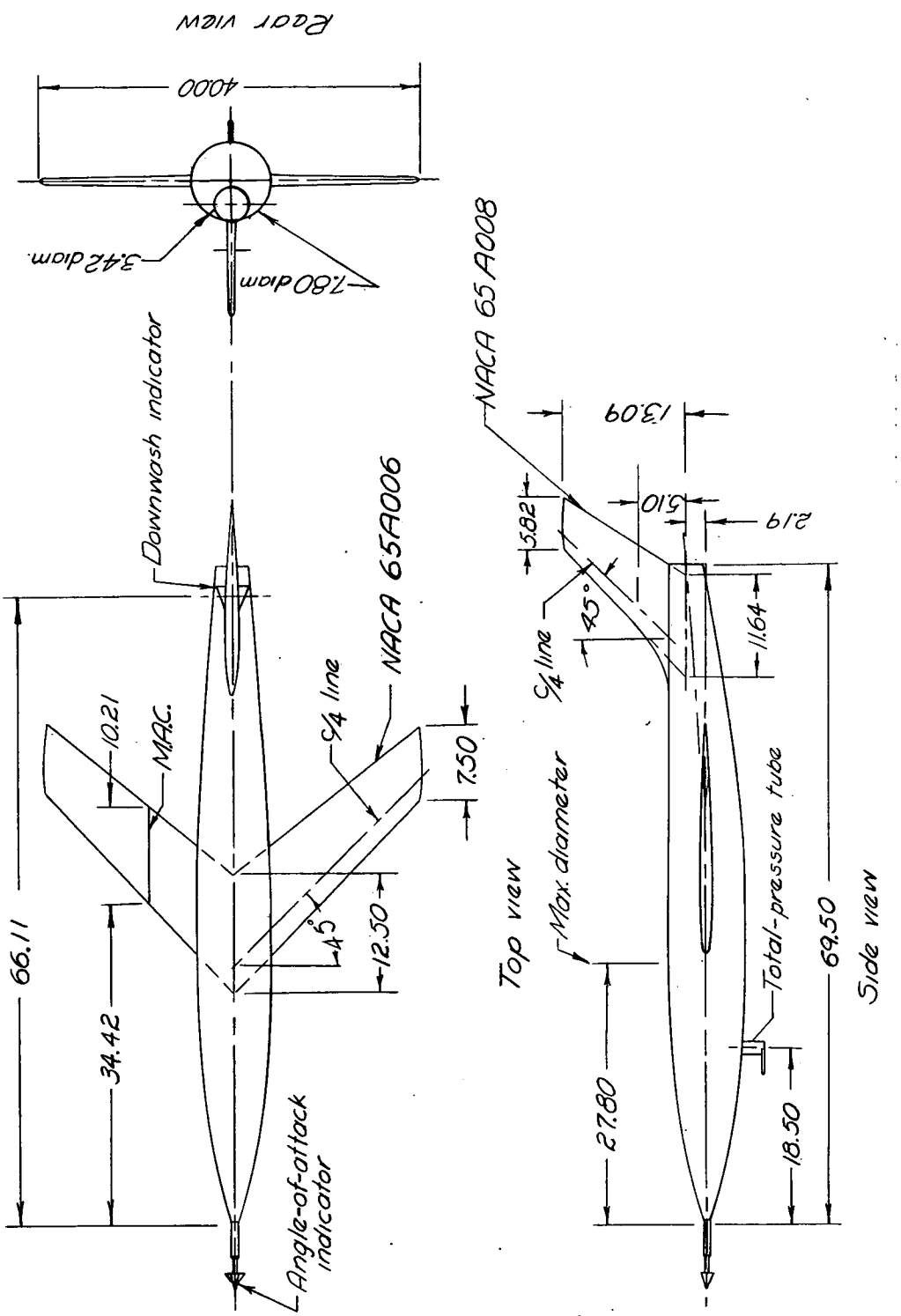

(b) Unsymmetric fuselage model.

Figure 1.- Concluded.

L-82842.1

Figure 2.- Model and booster combination in launching position.

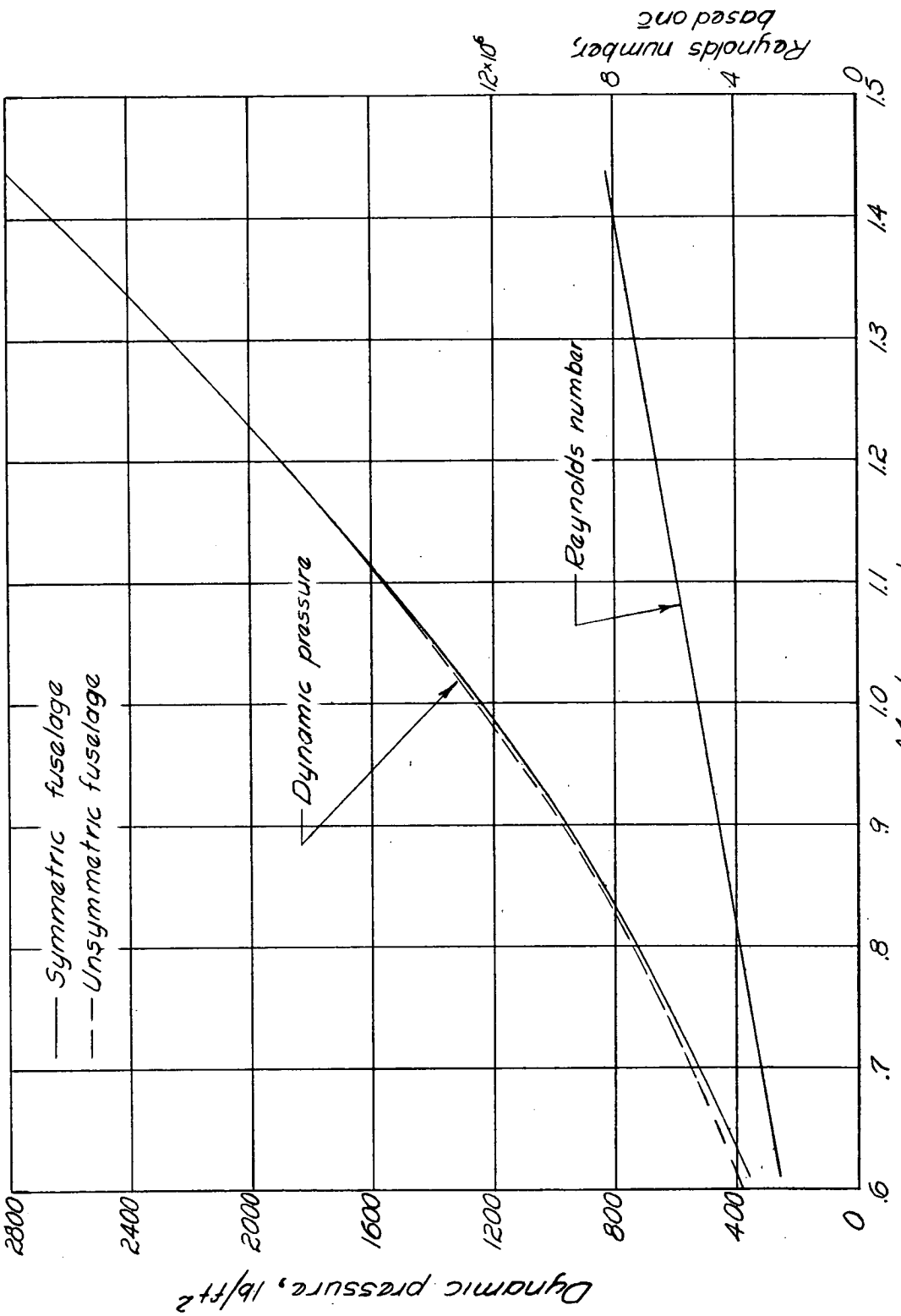

Figure 3.- Variations of dynamic pressure and Reynolds number with Mach number.

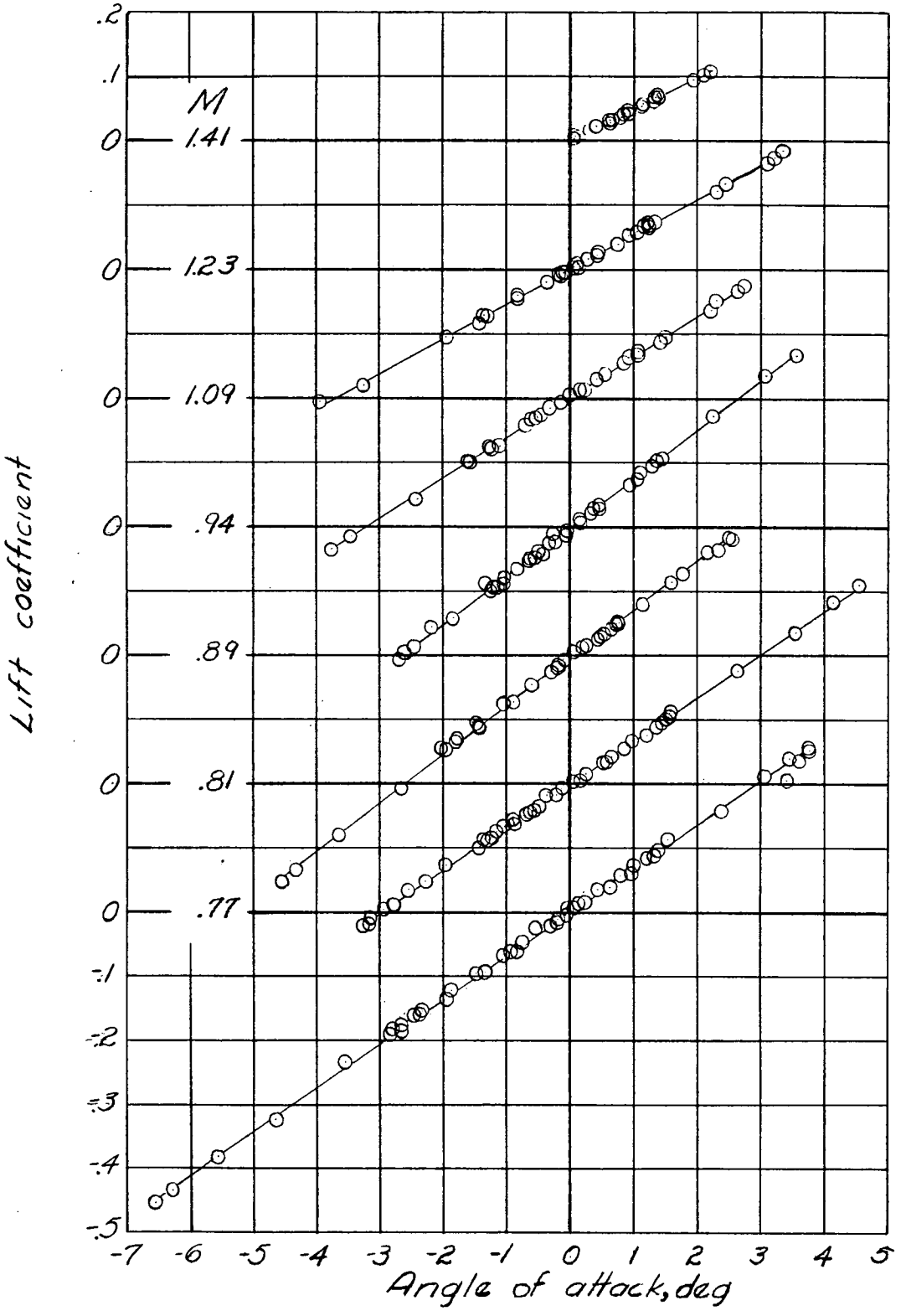

Figure 4.- Lift curves for symmetric model at several Mach numbers.

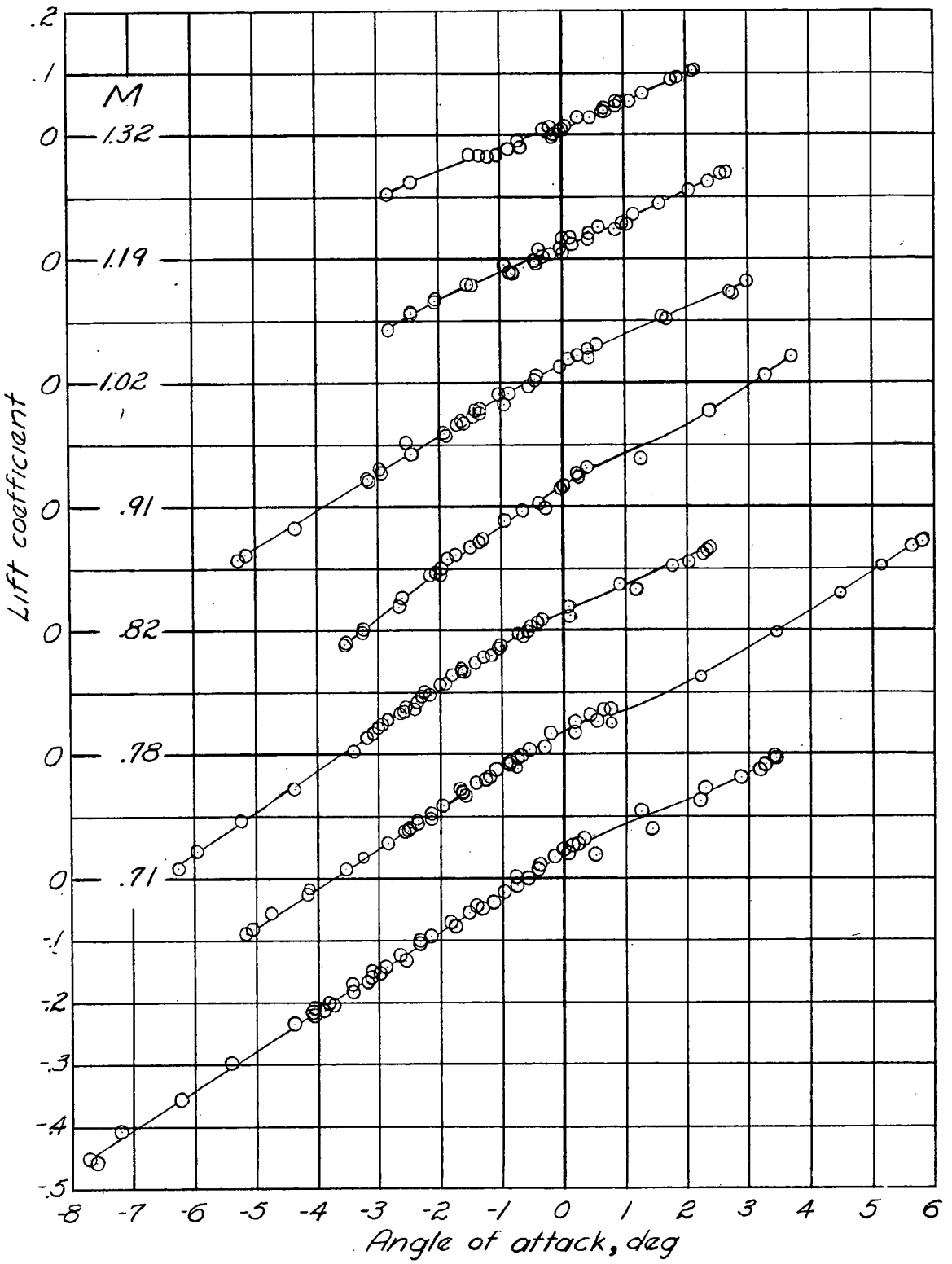

Figure 5.- Lift curves for the unsymmetric model at several Mach numbers.

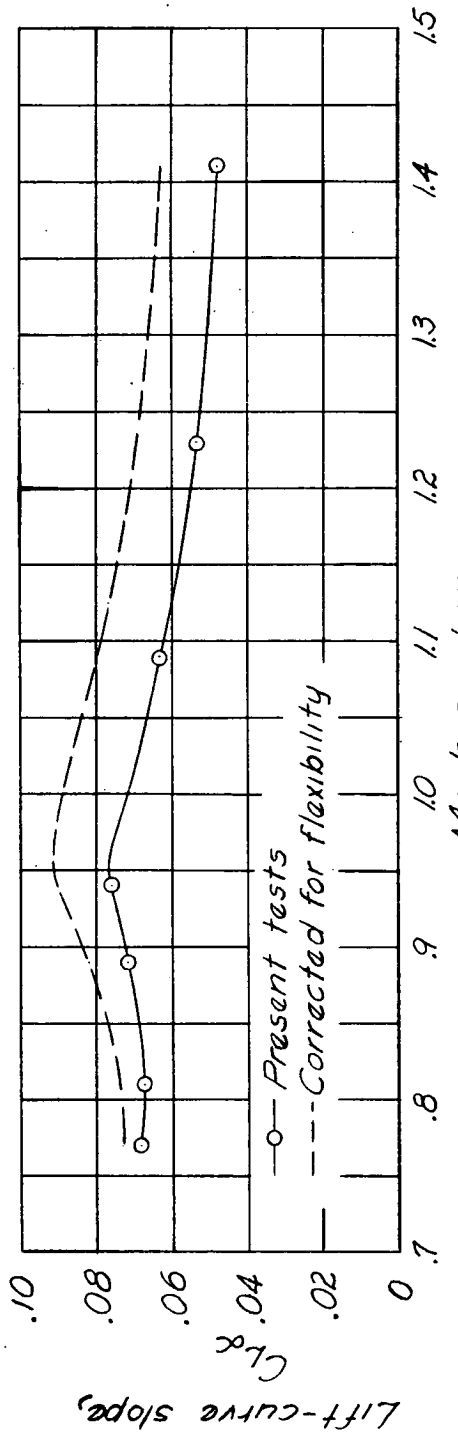

(a) Symmetric fuselage.

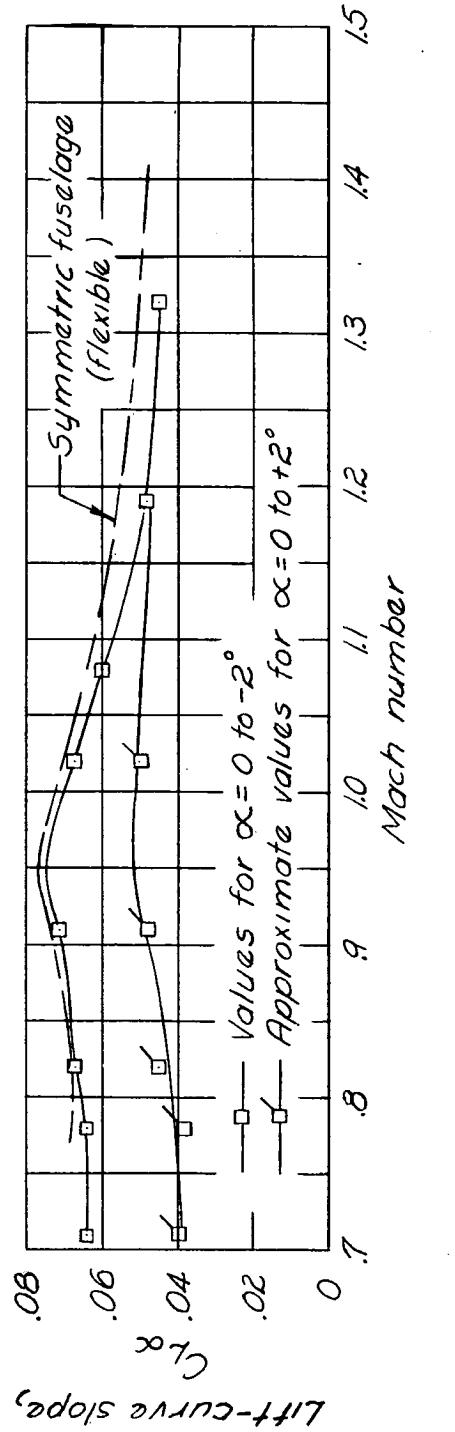

(b) Unsymmetric fuselage.

Figure 6.- Variation of lift-curve slopes with Mach number.

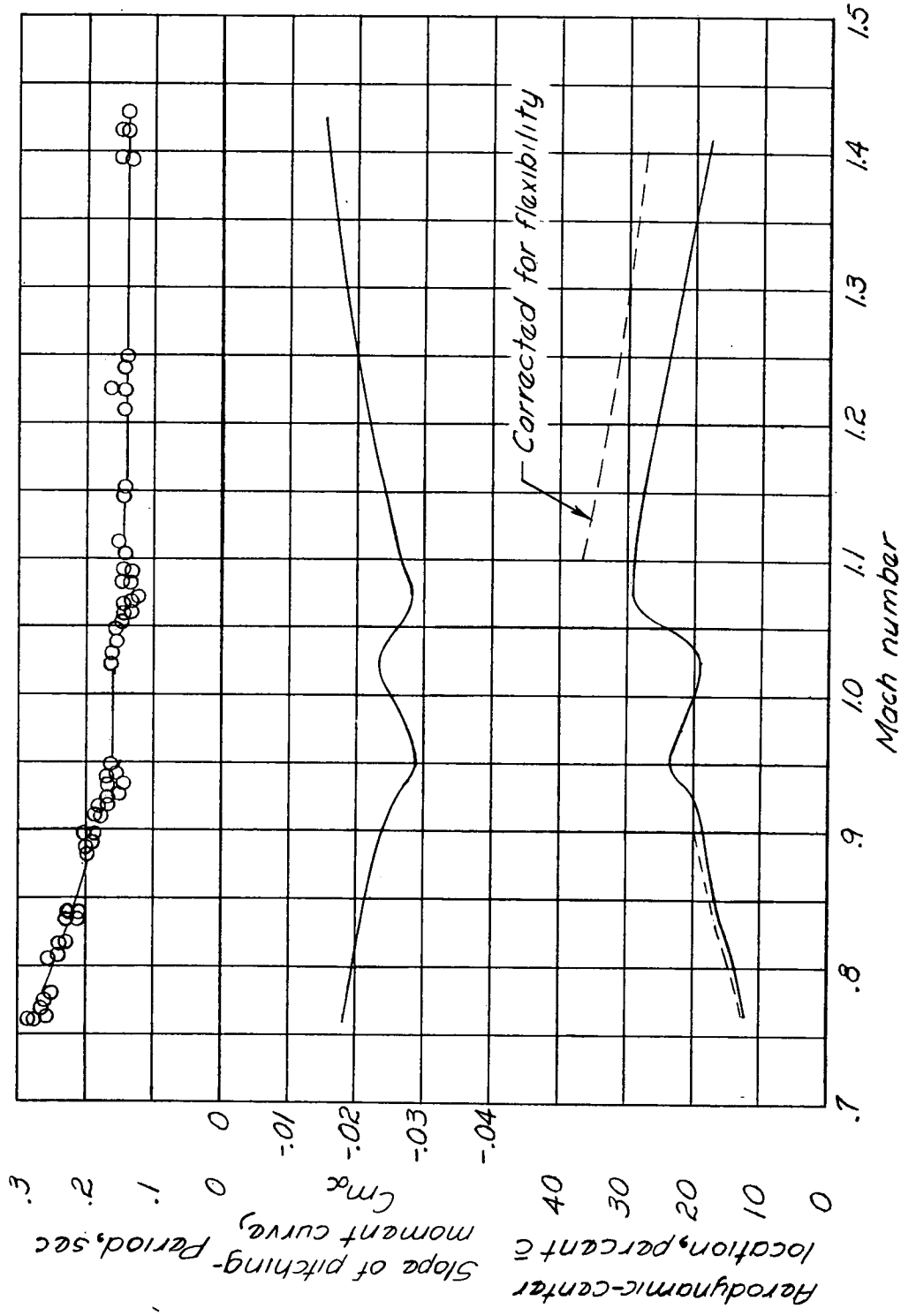

Figure 7.- Static longitudinal stability characteristics of the symmetric model. Center of gravity located at -14.4 percent $\bar{c}$.

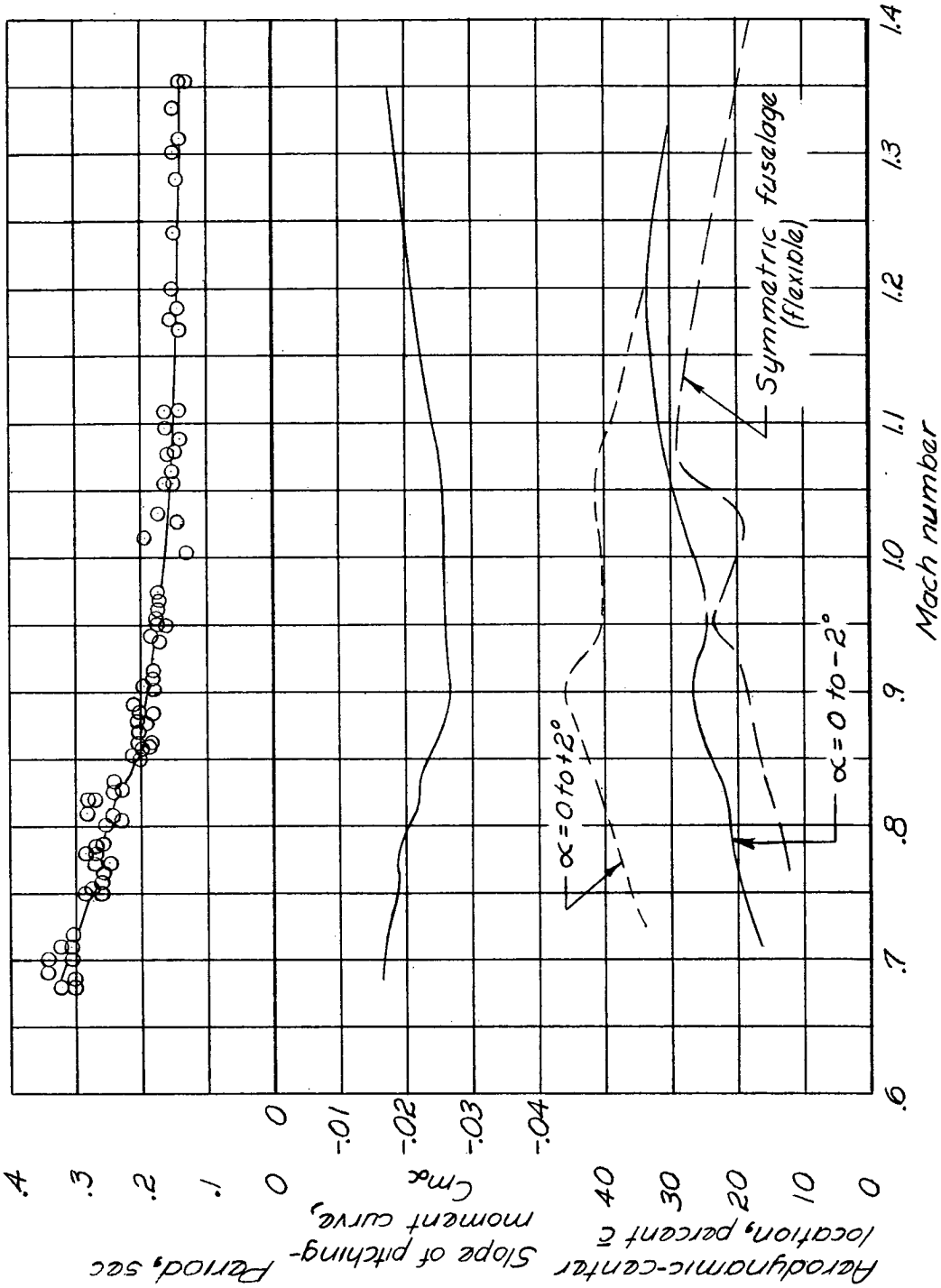

Figure 8.- Static longitudinal stability characteristics of the unsymmetric model. Center of gravity located at -10.2 percent c̄.

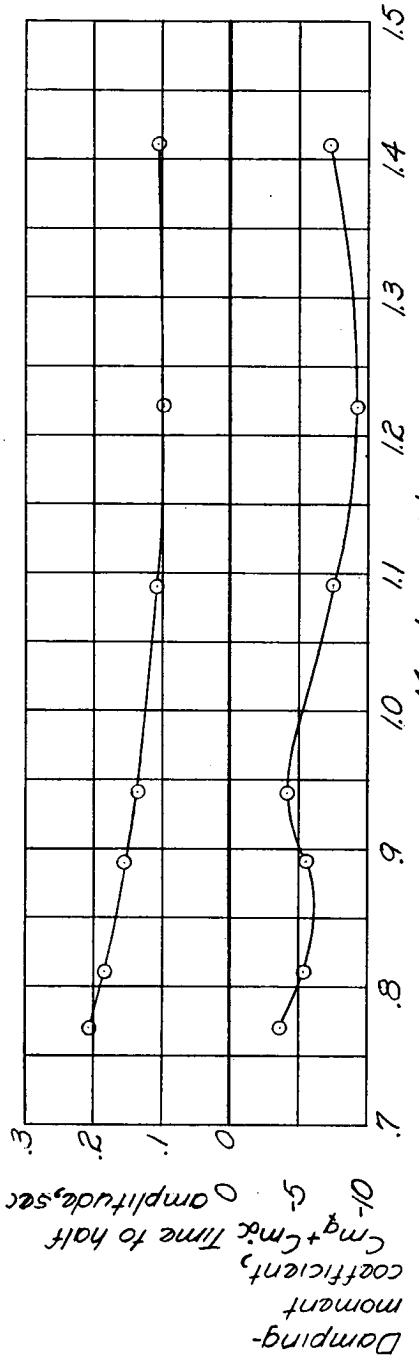

(a) Symmetric fuselage, c.g. at -0.144$\bar{c}$.

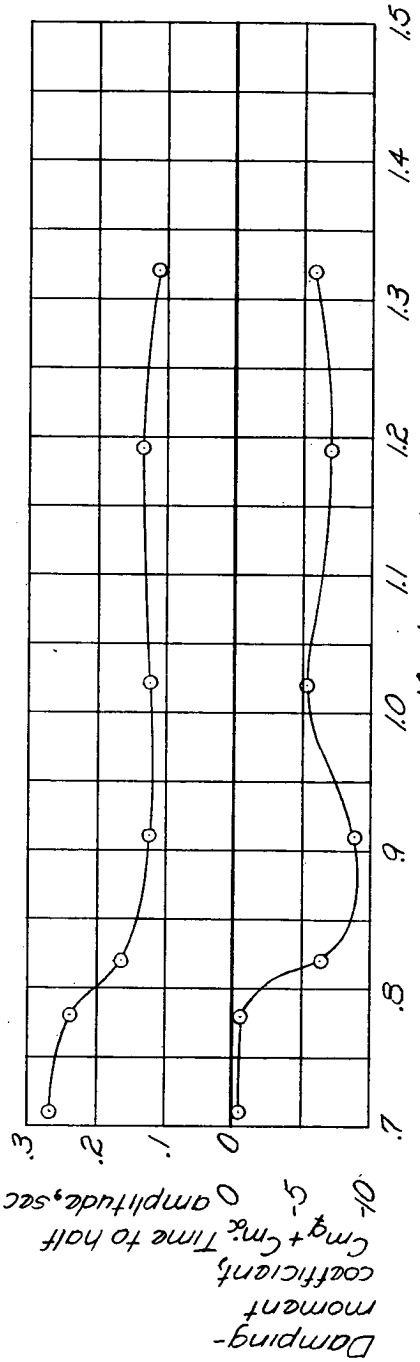

(b) Unsymmetric fuselage, c.g. at -0.102$\bar{c}$.

Figure 9.- Dynamic longitudinal stability characteristics of the models.

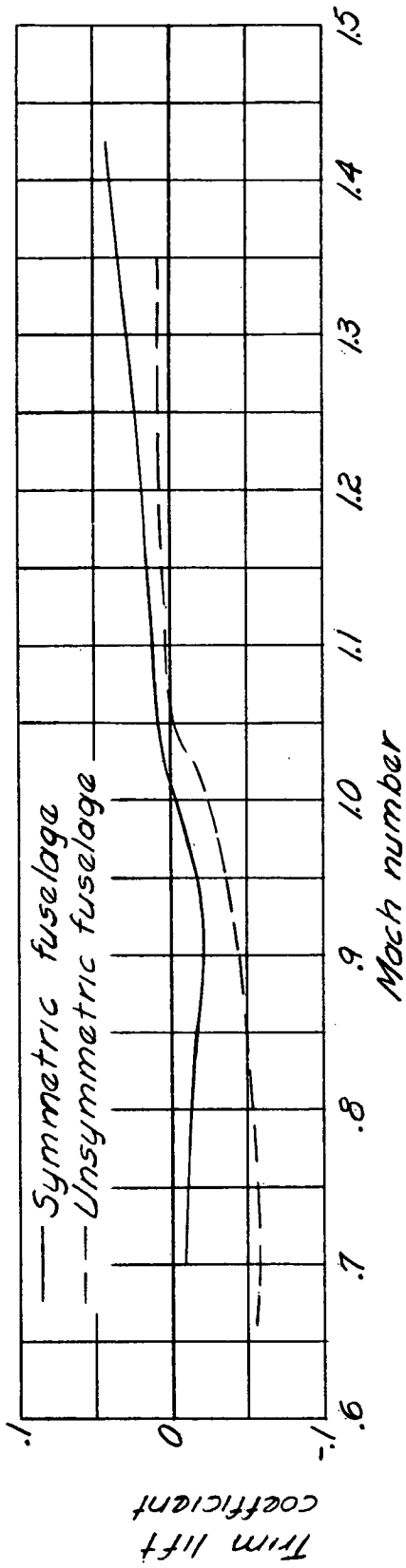

(a) Variations of trim lift coefficients.

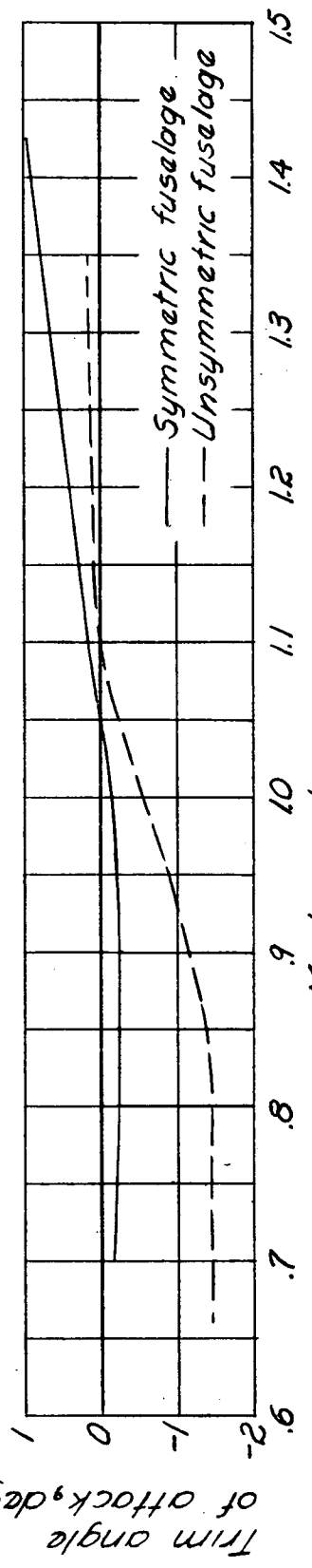

(b) Variations of trim angles of attack.

Figure 10.- Longitudinal trim characteristics of the models.

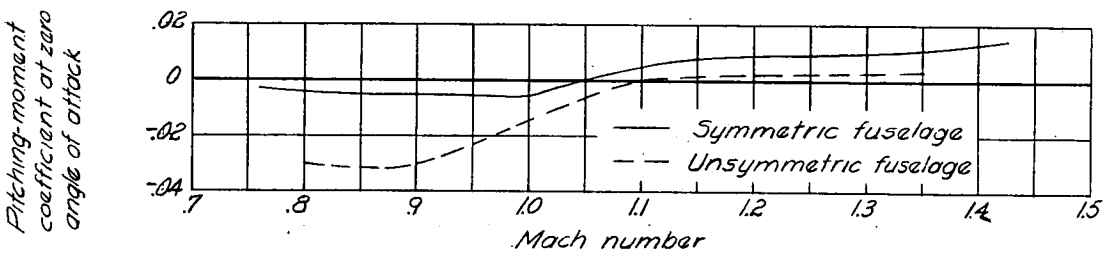

(a) Total model pitching-moment coefficients.

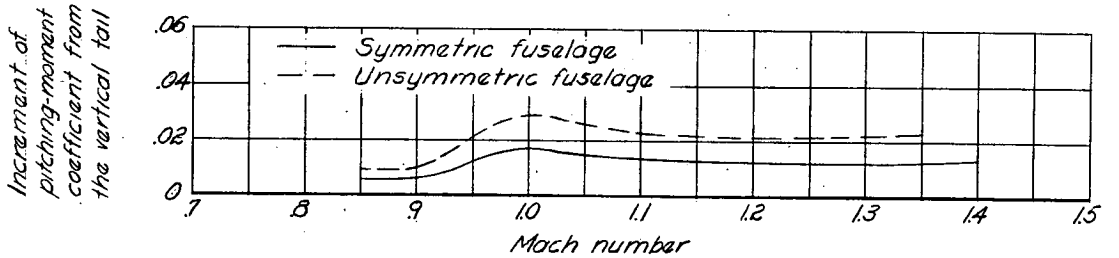

(b) Increment of pitching-moment coefficient due to drag of vertical tail.

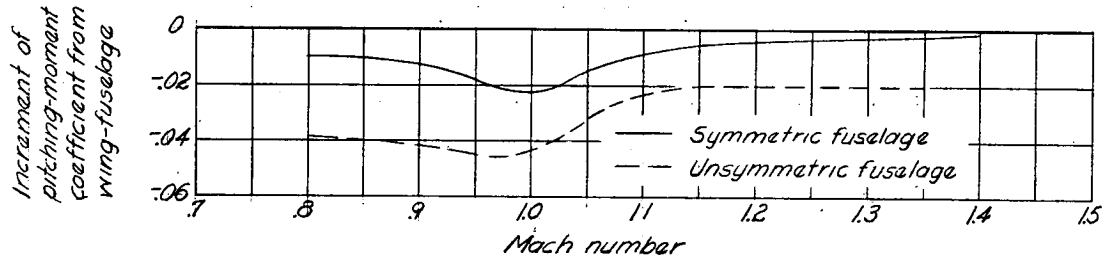

(c) Wing-fuselage pitching-moment coefficients.

Figure 11.- Variations of pitching-moment coefficients at zero angle of attack.

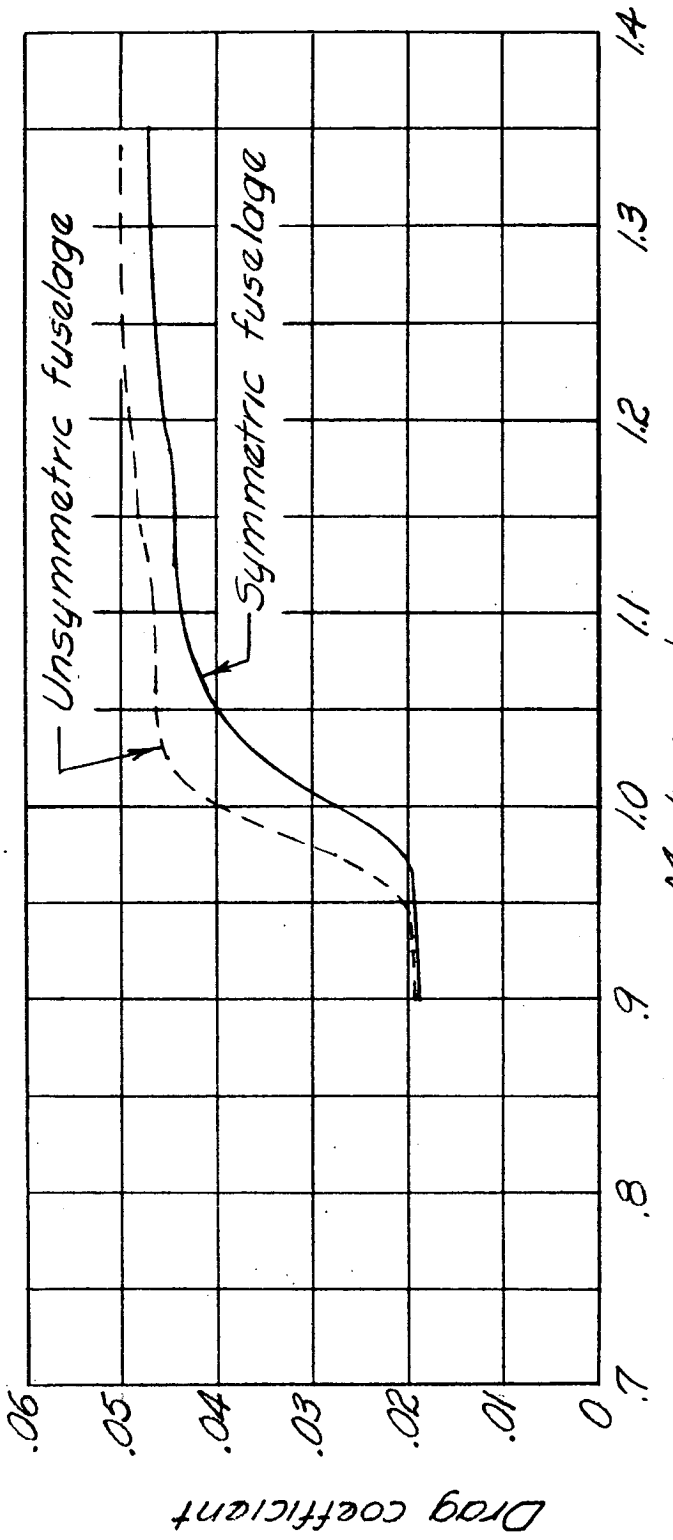

Figure 12.- Variations of drag coefficient at trim lift with Mach number.

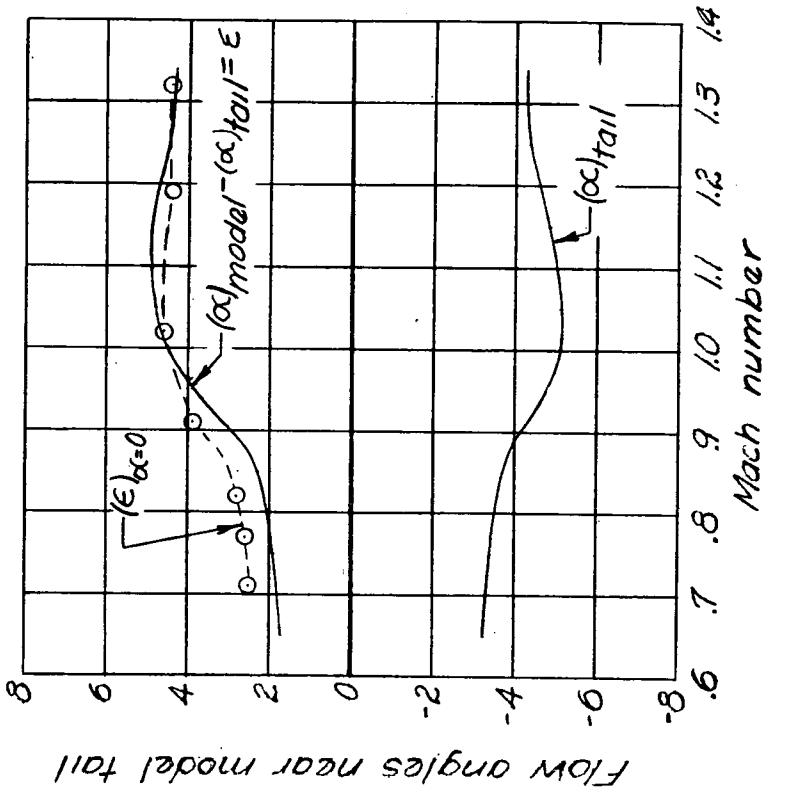

(a) Symmetric fuselage.

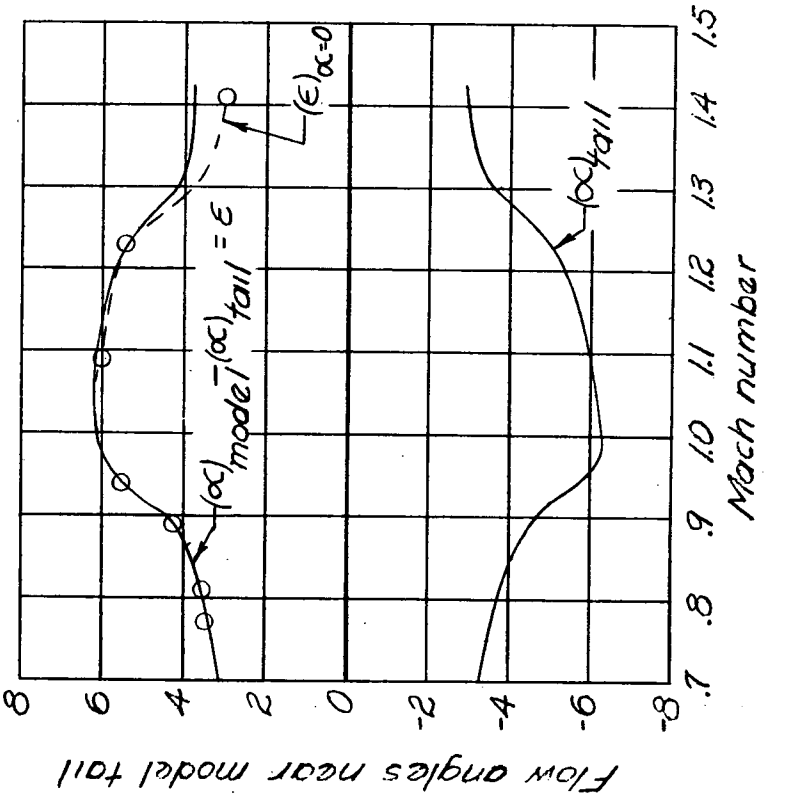

(b) Unsymmetric fuselage.

Figure 13.- Comparison of measured flow angles and downwash angles at trim lifting conditions.

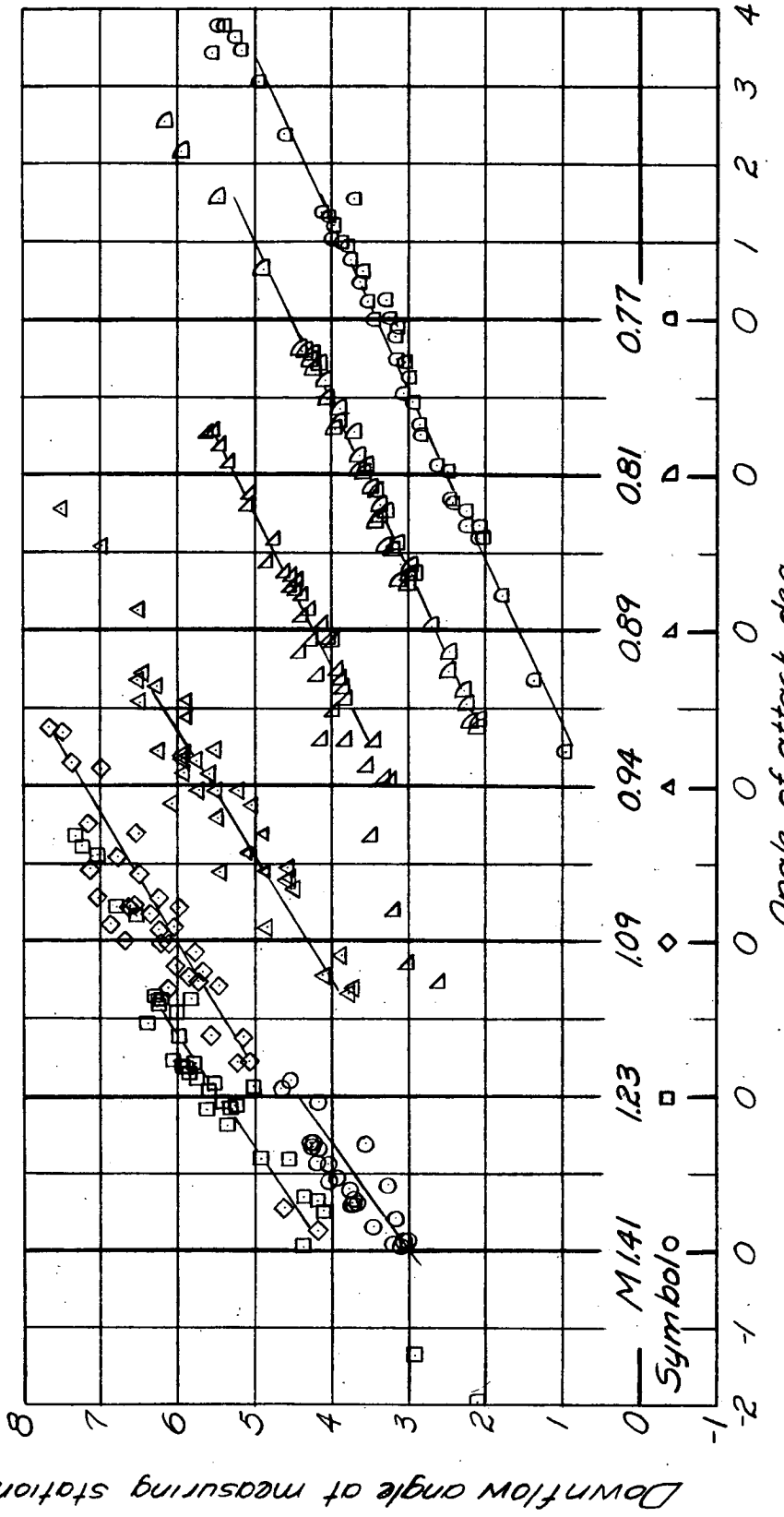

Figure 14.- Variation of downflow angle with angle of attack at several Mach numbers for the symmetric model.

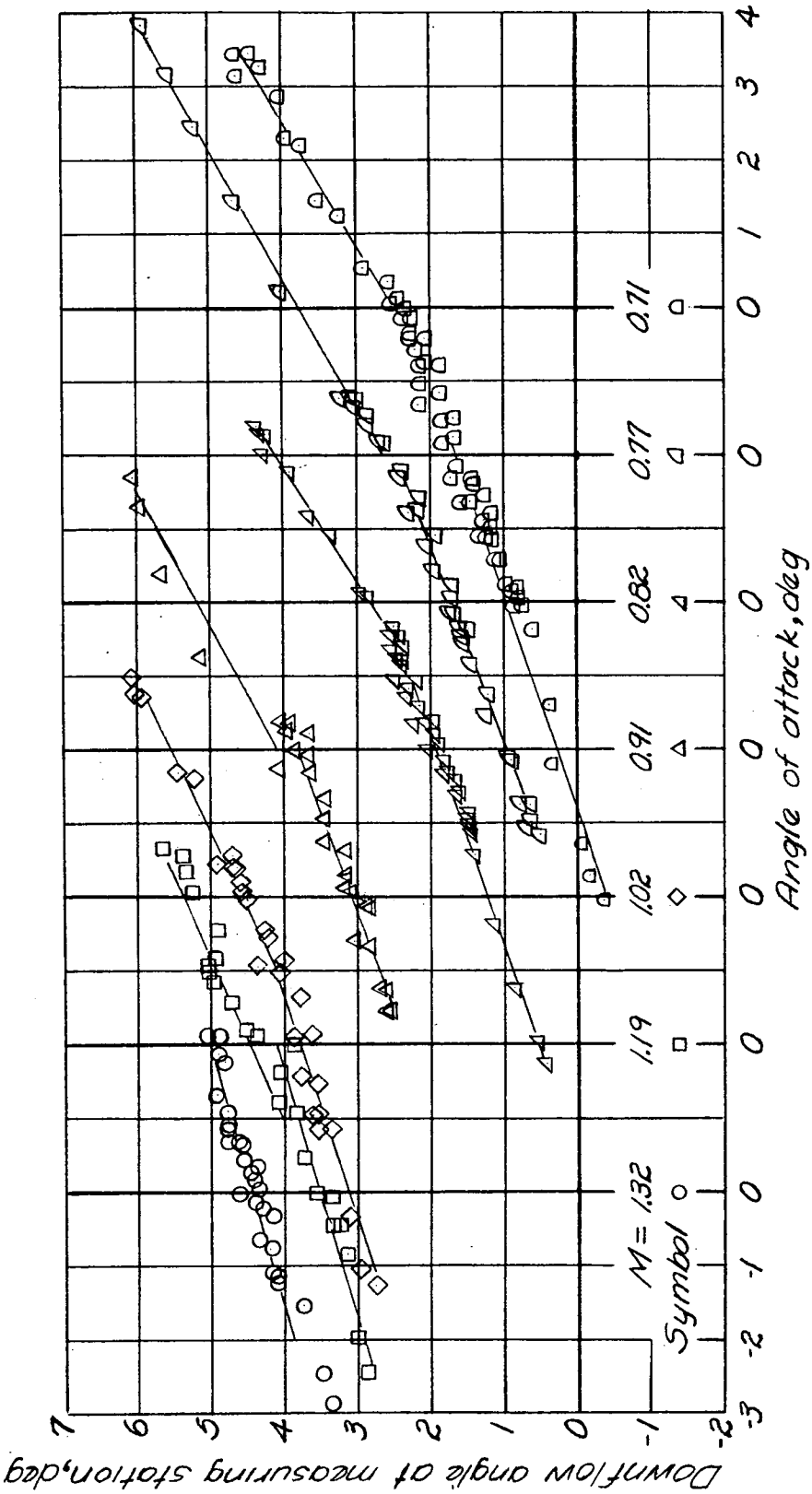

Figure 15.- Variation of downflow angle with angle of attack at several Mach numbers for the unsymmetric model.

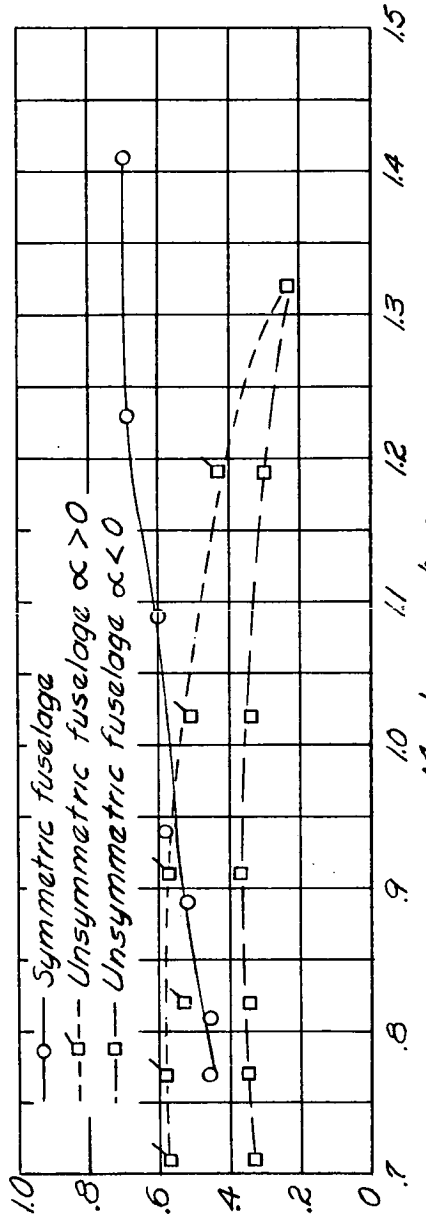

(a) Slope of downflow with angle of attack.

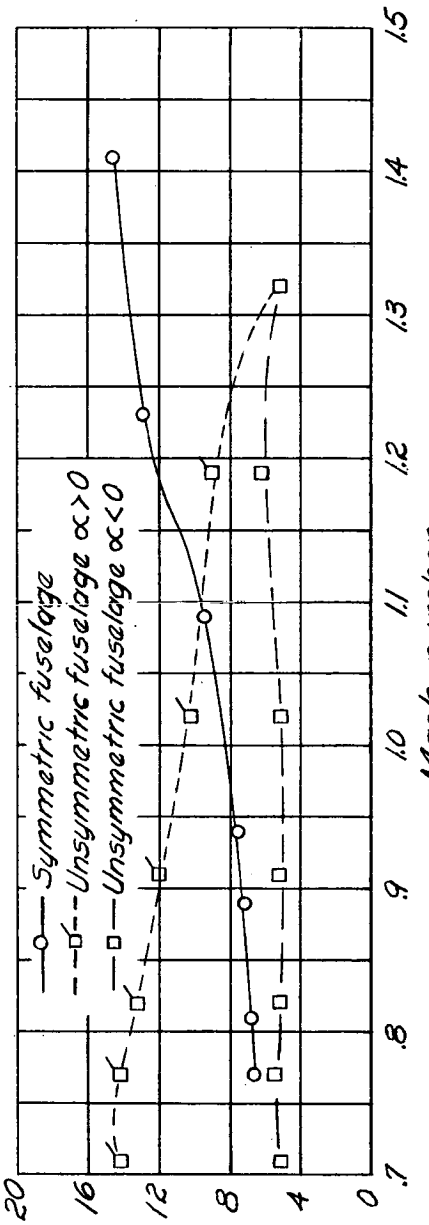

(b) Slope of downflow with lift coefficient.

Figure 16.- Variations of downflow slopes with Mach number.

NACA-Langley - 1-20-55 - 350